IEEE Photonics Journal
An IEEE Photonics Society Publication

Open Access

Switchable Multiwavelength Brillouin–Raman Fiber Laser Utilizing an Enhanced Nonlinear Amplifying Fiber Loop Design

Volume 10, Number 2, April 2018

Ghazaleh Mamdoohi, ***Member, IEEE***
Abdul Rahman Sarmani
Muhammad Hafiz Abu Bakar, ***Member, IEEE***
Mohd Adzir Mahdi

Graphic abstract

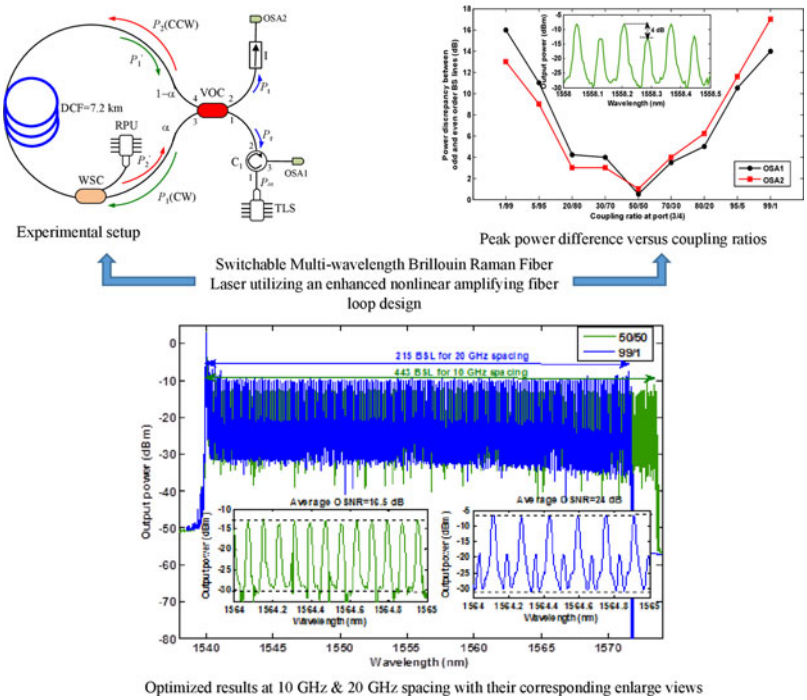

Optimized results at 10 GHz & 20 GHz spacing with their corresponding enlarge views

DOI: 10.1109/JPHOT.2018.2809557

Switchable Multiwavelength Brillouin–Raman Fiber Laser Utilizing an Enhanced Nonlinear Amplifying Fiber Loop Design

Ghazaleh Mamdoohi,[1] ***Member, IEEE***, **Abdul Rahman Sarmani**,[2] **Muhammad Hafiz Abu Bakar**,[1] ***Member, IEEE***, **and Mohd Adzir Mahdi** [1]

[1]Wireless and Photonics Network Research Centre, Faculty of Engineering, Universiti Putra Malaysia UPM Serdang 43400, Malaysia
[2]Department of Physic, Faculty of Science, Universiti Putra Malaysia UPM, Serdang 43400, Malaysia

DOI:10.1109/JPHOT.2018.2809557

Manuscript received December 16, 2017; revised February 9, 2018; accepted February 20, 2018. Date of publication February 27, 2018; date of current version March 22, 2018. This work was supported in part by the Royal Society-Newton-Ungku Omar under Advanced Fellowship Scheme, NA150463.
Corresponding author: Abdul Rahman Sarmani (e-mail: abdul.sarmani@yahoo.com.my).

Abstract: We propose and demonstrate a new multiwavelength Brillouin–Raman fiber laser with switchable 10 and 20 GHz spacing. This is achieved by proper adjustments of optical coupling ratios that are incorporated in the design that consists of an enhanced nonlinear amplifying fiber loop. By utilizing a 50/50 coupler, 443 flat amplitude channels with 10 GHz spacing is realized. On the other hand, a 99/1 coupler is feasible for 20 GHz spacing that yields 215 lasing lines. In both cases, the average optical signal-to-noise ratios (OSNR) are 16.5 dB (50/50 coupler) and 24 dB (99/1 coupler). Wide multiwavelength bandwidth, flexible wavelength spacing, and high number of channels with excellent OSNRs are achieved using only a single Raman pump unit through a simple construction.

Index Terms: Brillouin scattering, fiber laser, Raman Scattering.

1. Introduction

The exploitation of nonlinear optical effects has been utilized efficiently in the construction of multi-wavelength fiber lasers [1]–[4]. Amongst these, the Brillouin-Raman effect has been regarded as one of the best solutions with several important advantages [5]–[8]. These include stable multi-wavelength operation at room temperature with extremely broad workable wavelength band. A number of attempts have been carried out to optimize the performances of multi-wavelength Brillouin-Raman fiber laser (MBRFL) especially number of channels [6], [7] and flat-amplitude bandwidth [5], [9], [10]. Other important characteristics of concern are optical signal-to-noise ratio (OSNR) [11], [12], channel spacing [6], [13]–[15], and stability [16]. Nevertheless, one of the major challenges is to achieve uniform Stokes lines over a wider bandwidth domain [9]. Although utilizing multiple Raman pump sources is a feasible method of achieving this, it introduces higher cost and complexity. Wang *et al.* managed to circumvent this issue by utilizing only a single Raman pump unit when combining the active dispersion compensating fiber (DCF) as the Brillouin-Raman gain medium

together with the passive single mode fiber (SMF) [5]. The additional spectral reshaping scheme introduced by the latter fiber is employed to enhance the Rayleigh scattering effect on the Stokes comb. This leads to the generation of over 500 Stokes lines at 10 GHz spacing. However, the need for a tunable and flat amplitude bandwidth becomes more crucial with the advent of wider-spaced MBRFL.

In our earlier work that implemented an 11 km length DCF with an inclusion of 30 cm strand Bismuth-Erbium-doped fiber [6], a MBRFL with 20 GHz spacing is reported which yields 195 Stokes lines with 26 dB OSNR. In the same setup that employs only 7.2 km length DCF [7], investigations on Raman pumping distribution around Bi-directional and 100% forward directions are completed. In this case, the implementation of symmetrical coupler is the best choice when the optimization of 20 GHz spacing is the subject of main objective. This yields reasonably 212 flat amplitude channels with outstanding OSNR and Stokes peak power of 27.5 dB and -10 dBm correspondingly. However, previous researchers have also presented different discrete configurations for single and double wavelengths spacing [5]–[8], [10], [17]. This opens up the exploration of determining specific methods for acquiring multi-wavelength design flexibility and functionality within an individual architecture. Hence a MBRFL source with switchable wavelength spacing capability (10 and 20 GHz spacing) is highly desirable although this will inadvertently increase the difficulty of obtaining wider uniform bandwidth.

In order to resolve this conundrum, for the first time we propose a new cavity design that utilizes an enhanced nonlinear amplifying fiber loop (NAFL). This kind of configuration consists of a distributed Raman amplification medium inside a loop without employing any additional mirror at the end of the cavity. This is because the placement of a visible mirror inside the feedback mechanism, introduces 10 GHz spacing generation at all pump coupling ratios [8]. This favors exceptional performances around 300 mW pump power level, but leads to spectral broadening that deteriorates the OSNR quality at higher power scales. Instead of these, the NAFL utilizes Rayleigh scattering effects as a virtual mirror that tailors the generation of Brillouin Stokes lines (BSL) when pumping at a Watt power level. With reference to other earlier reports [5]–[8], the main achievements of this research work are not only to introduce novel improvements to number of channels, flatness, OSNR, and wavelength operation. Alternatively, the successful demonstration of the laser structure for switchable multi-wavelength operation for 10 and 20 GHz spacing in a single device footprint is the main interest. This is best described with the specific selection of 50/50 and 99/1 couplers at optimum values of Brillouin pump (BP) power, BP wavelength, and Raman pump power (RPP).

2. Experimental Setup

The schematic diagram of the MBRFL structure that incorporates an enhanced NAFL is outlined in Fig. 1. Its main element of pumping separation as represented by the variable optical coupler (VOC) is realized by incorporating a set of single-mode fiber component that individually introduces different fixed coupling ratios, CR. These are done by dividing the input signal coupling at port 3/4 with several proportions of 1/99, 5/95, 20/80, 30/70, 50/50, 70/30, 80/20, 95/5, and 99/1. The corresponding couplers are manufactured by Oplink communications and have return and directivity losses of more than 55 dB with different insertion losses with respect to their splitting ratios. For instance, a maximum of 3-dB loss is attributed to the 50/50 coupler and the rest indicates a lower loss than this value. The VOC essentially forms a fiber loop by including a 7.2 km long DCF. This specific fiber behaves as a hybrid Brillouin-Raman gain medium with a nonlinear coefficient of 7.3 $(\text{Wkm})^{-1}$ and an effective area of 20 μm^2. The wavelength selective coupler (WSC) is used to combine a 1455 nm Raman pump unit (RPU) that has a maximum power of 1000 mW to the nonlinear oscillator. In addition, the BP is provided by a tunable laser source (TLS) that has a 200 kHz linewidth. Its wavelength tunability varies from 1520 nm to 1620 nm and its output power range is from around -3 dBm to a maximum of 5 dBm. This device is coupled to the input port of the VOC through an optical circulator C_1. Moreover at another VOC fiber end, an isolator (I) is used to prevent any back-reflected signal into the NALF that might disrupt the stability of laser operation. No any visible feedback scheme is included next to this device in comparison to the

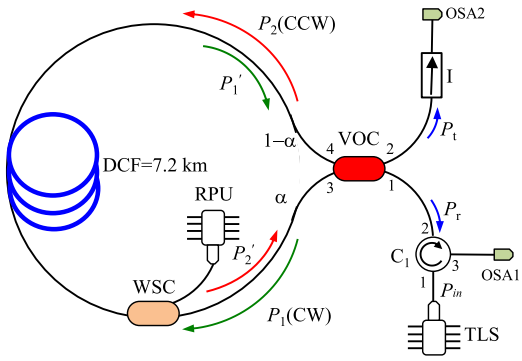

Fig. 1. Cavity design by utilizing an enhanced NAFL without a mirror next to the isolator. P_1 and P_2, P_t and P_r: Signal powers where indexes 1 and 2 indicate partial input beam and indexes t and r represent the transmitted and reflected output power respectively.

previous assessment [8]. The results obtained are evaluated by employing two optical spectrum analyzers (OSA1 and OSA2) with a resolution bandwidth of 0.02 nm at two different output terminals as depicted in Fig. 1.

3. Results and Discussions

Before initiating further discussions on the operation principles of the NAFL and the corresponding results, a brief theoretical investigation of this structure based on the nonlinear amplifying loop mirror (NALM) approach [18] is presented first. As the NALM concept already represents the foundation for NAFL functions, we only mention about the latter design for the whole discussion in this report. As mentioned earlier, the lasing feedback in NAFL is mainly initiated by Rayleigh scattering without the inclusion of any additional broadband mirror in the enhanced setup that is described in [8]. As shown in Fig. 1, an input signal from TLS (P_{in}) is injected to port 1 of the VOC and splitted by this component with the splitting ratio of $\alpha/(1-\alpha)$. This generates two partial signals with power levels for the clockwise (CW) beam, $P_1 = \alpha P_{in}$ and for the counter-clockwise (CCW) beam, $P_2 = (1-\alpha)P_{in}$. In the entire analysis, the numerator of CR denotes the fraction of power at port 3 and the denominator implies the fraction of power at port 4. Together with the inclusion of a Raman pump source, both signal powers of P_1 and P_2 counter-propagate through the DCF, thus experiencing distributed Raman amplification. In this case, the Raman laser serves as a forward pumping source for signal power P_1 such that the gain decreases along the fiber and it also acts as a backward pumping source for signal power P_2 in which the gain increases along the fiber. After a cavity round trip, these amplified interacting waves acquire different power levels through self-phase modulation (SPM) in the NAFL. This can be expressed as [18],

$$P_1' = \left(\sqrt{\alpha}A_{in}\exp\left(c_1 + i\alpha\gamma L_{eff,1}|A_{in}|^2\right)\right)^2,$$
$$P_2' = \left(\sqrt{(1-\alpha)}A_{in}\exp\left(c_2 + i\left(1-\alpha\right)\gamma L_{eff,2}|A_{in}|^2\right)\right)^2, \quad (1)$$

where the relation between the Brillouin input power to the amplitude is given as $P_{in} = |A_{in}|^2$, γ is the nonlinear (Kerr) parameter of the fiber, $C_{1,2}$ and $L_{eff,1,2}$ are the loss-gain profiles along the propagation distance, z [18]. In (1), the subscripts 1 and 2 in this theorem are associated with the properties of P_1 and P_2 respectively. More elaborations on these mathematical symbols are given in [8, eq. (2)–(5)]. In fact, the signal-induced cross phase modulation in the loop is ignored because the RPP is substantially larger than the signal power in practice. Since the continuous wave input signal with a 200 kHz linewidth is used, the incorporating negative dispersion of DCF and SPM do not satisfy the Schrodinger equation for the soliton effects [19]. Hence for simplification, the effects

of negative dispersion in (1) are ignored. As a result, the solution of this equation is straightforward and the effect of SPM on the propagating signals is the only factor considered.

Once light bouncing back and forth in a cavity round trip is completed, the signals P_1' and P_2' with different power intensities recombine interferometrically at the coupler. This yields the nonlinear output properties of transmitted and reflected beams, P_t and P_r as well as phase shift characteristic. As a result, the intensity imbalance in the loop is mostly proportional to the Raman amplification effect according to their corresponding splitting ratio. So from above explanation (1), it is evident that for a splitting ratio that ranges from 1/99 to 10/90 ($\alpha = 0.01$ to 0.1) the power of P_1' is lower compared to that of P_2'. Therefore, P_2' is more sensitive to the power-dependent nonlinear phase difference and mainly determines whether the interference at the output coupler is constructive or destructive. As P_1' role is not considerable although its phase is changed by SPM, P_2' also governs the power and the phase shift of the output signal. Interestingly, for coupling ratios of 20/80, 30/70, 40/60, 60/40, 70/30, and 80/20 both amplified counter-propagating signals affected by SPM determine the values of P_t and P_r, as well as the phase of an output signal. For another case of CR $=$ 50/50, the discrepancy among counter-propagating signals is not as significant as other coupling ratios. The reduction in the phase shift is realized since the power discrimination between P_1' and P_2' is weaker, thus resulting in the minimum interference. These parameters explain the possible selection of this coupler for 10 GHz spacing generation. Alternatively, for CR that covers from 90/10 to 99/1 ($\alpha = 0.90$ to 0.99), P_1' is the main decisive factor in the phase shift values as well as output power. It is noted that when a stronger CW signal with a power ratio αP_{in} is co-pumped with the Raman laser source, it experiences lower loss compared to the CCW signal. Although the Raman gain profile for the weaker CCW signal increases along the fiber length, its power is low due to higher propagation loss along the fiber compared to that of the CW signal. As the SPM effects are enhanced for a stronger signal, a higher intensity mismatch is initiated. This results in more phase differences among the interacting waves as well as stronger destructive interference at the coupler which justifies the maximum level of phase shift at 99/1 coupler. As a result, this might be feasible for the 20 GHz. spacing operation. So we can conclude that the splitting ratio is a crucial factor for the output power and phase characteristics. This is because the differential Raman amplification, splitting ratio α , as well as input power P_{in} are responsible for an oscillatory behavior of the induced phase shift and alternative output power, P_{out} consisting of transmitted, P_t and reflected beam, P_r. The intensity imbalance in the loop is mostly proportional to the Raman amplified interacting signals according to their corresponding splitting ratio. The reduction of the phase shift is achieved at the expense of weaker power discrimination between counter-propagating signals (P_1' and P_2'). In contrast, the increase of the phase shift is associated to the higher intensity mismatch between both signals (P_1' and P_2'). Therefore in summary, the sensitivity of NAFL response to the splitting ratio implies different inherent interference characteristic inside the coupler, which offers the best exploitation of the wavelength spacing.

In order to verify our hypothesis, an experiment is carried out based on the laser configuration as depicted in Fig. 1. During experiment, the input BP power that is splitted by a coupler into two partial signals counter-propagates in the DCF and encounters Raman amplification. Once the stimulated Brillouin scattering (SBS) threshold power is satisfied, the two first-order Stokes signals are initiated in opposite directions with respect to the injected BP signals in the loop. As this process relies on the propagation direction, different Raman gains are induced that also result in different phase shifts due to the SPM effect. When the next threshold condition is met, they become two new BP sources that generate the second-order Brillouin Stokes signal (BSS) in similar directions to those of P_1' and P_2'. Simultaneously, the first-orders BSS also undergo Rayleigh backscattering effects that initiate a distributed feedback mirror. However, due to the intrinsic attribute of lower Raman gain for P_1', its Rayleigh parts of first-order BSS do not grow as much as those for the first-order BSS generated by P_2'. The generation of successive orders BSS within the accessible Raman amplification bandwidth continues to develop as long as the corresponding preceding orders reach their SBS threshold condition. These cascading effects are terminated when the total gain in the laser cavity cannot surpass the cavity loss at the operating wavelengths. In parallel to this effect, the Rayleigh backscattering phenomena are also initiated synchronously from the preceding orders BS

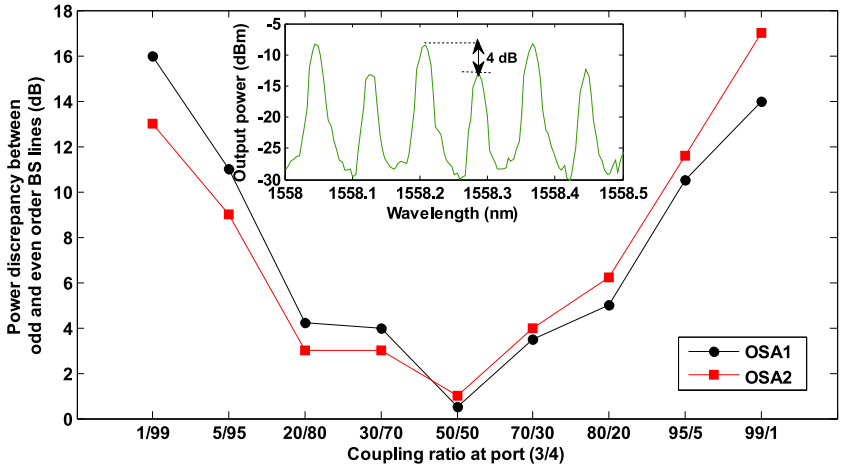

Fig. 2. Peak power difference between odd- and even-order BSL as a function of coupling ratio. The inset shows the output spectrum from the laser cavity with 20/80 CR at OSA2 (RPP = 1000 mW, BP wavelength = 1555 nm, BP power = 5 dBm).

waves. In this case, the first interaction between the first-orders BSS and their Rayleigh-scattered beams occur inside the fiber loop. This process continues to exist between the next-orders BSS with their corresponding Rayleigh-scattered beams. Consequently, the resulting spectra recombine inside the coupler and then separated into two partially transmitted and reflected portions with power of P_t and P_r respectively. For clarification, these output beams are the results of overlapping between multiple orders BS components circulating inside the cavity. Owing to this process, by proper adjustment of the CR, the phase shift between BS components in the coupler can be varied. This results in peak power discrepancies between the odd- and even-order lasing lines which determine the required multi-wavelength spacing.

To investigate the right coupling properties required to realize 10 and 20 GHz spacing with high number of channels and acceptable OSNR, the VOC is changed from 1/99 up to 99/1. Several pumping conditions are fixed throughout this experiment that includes RPP of 1000 mW and BP power of 5 dBm. This BP wavelength is maintained at 1555 nm as it corresponds to the Raman peak gain when the first shift is initiated from the original RPU wavelength of 1455 nm. The experimental results that indicate the peak power discrepancy between the neighboring channels along the entire laser-comb bandwidth are depicted in Fig. 2. It is important to explain clearly how these measurements are assessed by using the OSA with 0.02 nm resolution. First, all the relevant Stokes peak power (SPP) are converted from dBm to mW and their average values at each coupling ratio are calculated separately. These are then converted back to dBm where the difference between the odd- and even- order lasing channels is evaluated from their average values in dBm as shown by the inset graph in Fig. 2. In this case, the achievement of 10 and 20 GHz wavelength spacing is defined as follows. A single wavelength spacing (10 GHz) in the spectral envelope is defined by including all lasing lines that have peak power discrepancies within 3-dB range. From this Fig., the couplers of 50/50 and 70/30 may satisfy this specification, but the symmetrical one is more favorable. These power differences grow bigger when utilizing other asymmetrical couplers due to their stronger phase difference. Moreover in order to attain the highest peak power discrepancies, the employment of 1/99 and 99/1 coupling ratios are suggested. This is the main criterion to satisfy the condition for generating double-wavelength spacing (20 GHz). However, a slight difference in power discrepancy at port 1 and port 2 as represented by black and red lines in Fig. 2 is observed. This might be due to the degree of tolerance of the output coupling ratio and dynamics of the interference that occurs among the corresponding waves. Furthermore, as the 99/1 coupler has a maximum of 17 dB peak power difference at port 2, it is chosen for further analysis of 20 GHz spacing operation as suggested earlier from the theoretical prediction.

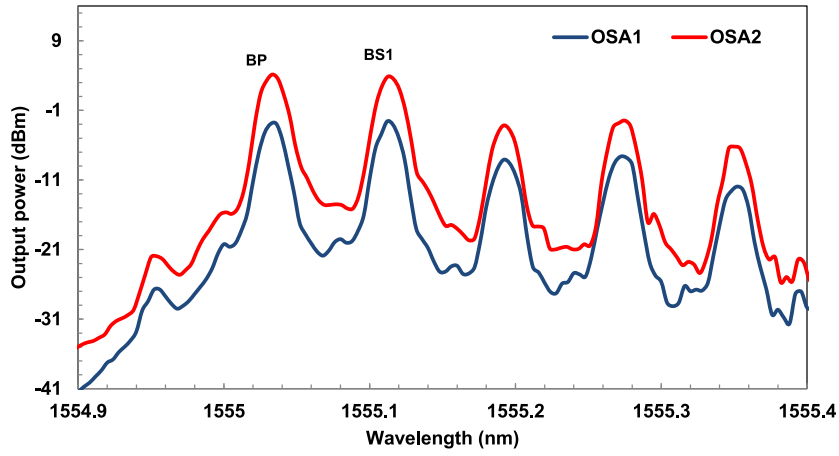

(a)

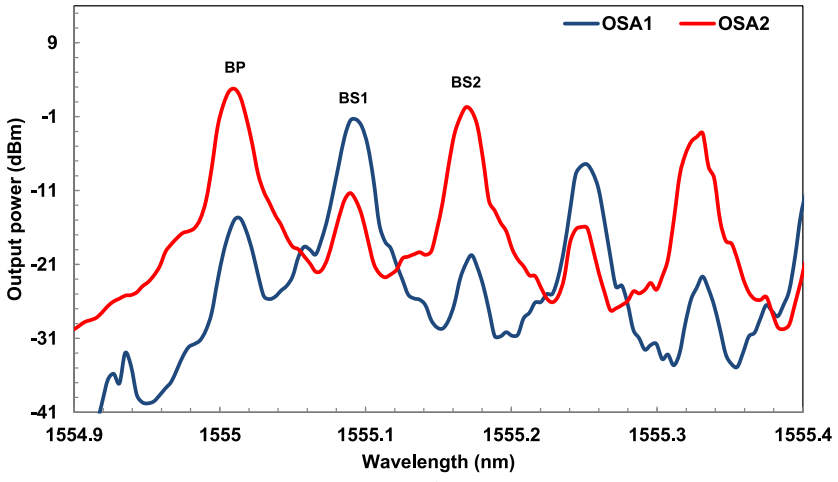

(b)

Fig. 3. Spectral profiles monitored at multiple locations for (a) 10 GHz and (b) 20 GHz spacing. BP is the Brillouin pump, BS1 is the first-order and BS2 is the second-order BS (RPP = 1000 mW, BP wavelength = 1555 nm, BP power = 5 dBm).

To further understand the effect of multiple interferences between the interacting spectra, two contrasts that represent different wavelength spacing at two couplers of 50/50 and 99/1 are selected from Fig. 2. In this case, the same pumping characteristics are used and the output spectra monitored at OSA1 and OSA2 are shown by blue and red lines in Fig. 3, respectively. When the 50/50 coupler is employed, both counter-propagating signals are strong enough with a relatively small phase difference. As the first- and higher-orders BS components are generated in both directions, interference with very small difference occurs inside the coupler. This results in the generation of 10 GHz spacing as demonstrated by the resulting spectra in Fig. 3(a). In contrast by utilizing the 99/1 coupler, a larger portion of first-order BS component emits from port 1 and that of a smaller fraction at port 2, VOC. When the next threshold is fulfilled, an inverse phenomenon occurs where a larger portion of second-order BS component is accumulated at port 2 (OSA2) while a smaller fraction is transferred to port 1 (OSA1). As a result, the spectrum at OSA2 consists of even-orders attribute when those of odd-orders are generated at OSA1 as elucidated in Fig. 3(b). When these sequential coherent BS components interfere at the coupler with high phase difference, the semi-destructive interference among them leads to the generation of 20 GHz spacing. Next, the relation of these couplers to the OSNR is assessed when the RPP increments are determined from

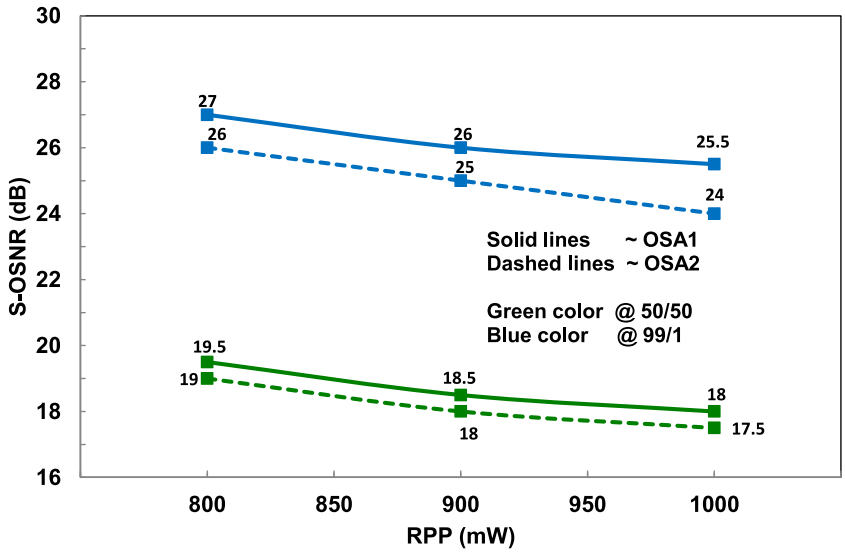

Fig. 4. Average OSNR values versus RPP variation at optimum coupling ratios (BP power = 5 dBm, BP wavelength = 1555 nm).

800 to 1000 mW as shown in Fig. 4. This power range is chosen since the higher RPP provides a sufficient energy transfer from the BP to its BSS. For clarification, the average value of OSNR along the flat spectral bandwidth is evaluated by including all lasing lines that have discrepancies in peak power of less than 3-dB span [7]. The same method is used when counting the numbers of lasing lines, degree of flatness, and multi-wavelength bandwidth as will be discussed in details later. In this assessment other pumping characteristics, especially BP power and BP wavelength are maintained at similar preliminary values. From Fig. 4, it can be inferred that with the increase in RPP, the average OSNR is reduced gradually for both CRs. This trend is influenced by the rising noise floor at higher RPP that is associated to the spectral broadening phenomenon on each lasing line caused by turbulent waves [20]. From this Fig., the maximum average OSNR for 99/1 coupler is 27 dB at port 1 before decreases slightly to 26 dB at port 2 when the RPU is set at 800 mW. On the other hand for 50/50 coupler, OSNR values also indicate a small reduction within 0.5 dB-range from the original 19.5 dB-level at OSA1 when referring to the signals at OSA2. Also when the RPU is set at 1000 mW, the maximum average OSNR is 18 and 25.5 dB for 50/50 and 99/1 couplers at port 1, respectively. The OSNR reductions between 0.5 dB and 1.5 dB are measured at another port. Therefore from the results obtained, the attainment of efficient single- and double-wavelength spacing with excellent OSNR qualities can be realized when the spectra are taken from port 1 (OSA1) at all RPP values. Owing to this fact, the next analysis is focused solely on data acquired at OSA1.

In order to obtain the highest number of BSL with a high OSNR, the optimization of injected BP power and RPP is also carried out as shown in Fig. 5. With reference to the previous assessment explained in Fig. 4, the RPP range and BP wavelength are fixed at the same values while the BP power is changed from −2.6 to 5 dBm. The results obtained demonstrate that the number of Stokes lines increase with the RPP increment due to the higher energy transference from the RPU to the BP power for both coupling ratios. In contrast, the reduction number of Stokes line is observed by increasing the BP power from −2.6 to 5 dBm. In this case, when the RPP is set at 1000 mW the number of lines decline from 216 to 206 and 110 to 91 lines for both couplers of 50/50 and 99/1 respectively. This can be attributed to the optimization of Raman gain at lower BP power where its gain saturation is fulfilled faster at higher BP values.

In Fig. 6, the relationships between BP wavelengths with the number of Stokes lines and multi-wavelength bandwidths are investigated. The RPP is fixed at 1000 mW and the BP power is

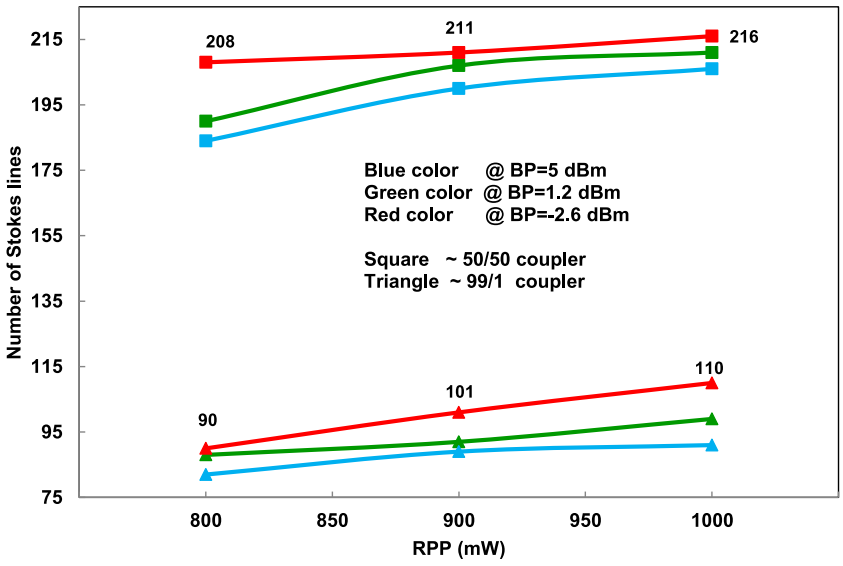

Fig. 5. Number of channels versus RPP for coupling ratio of 50/50 and 99/1 as measured at OSA1. The BP wavelength is maintained at 1555 nm and the BP power is set to −2.6, 1.2, and 5 dBm.

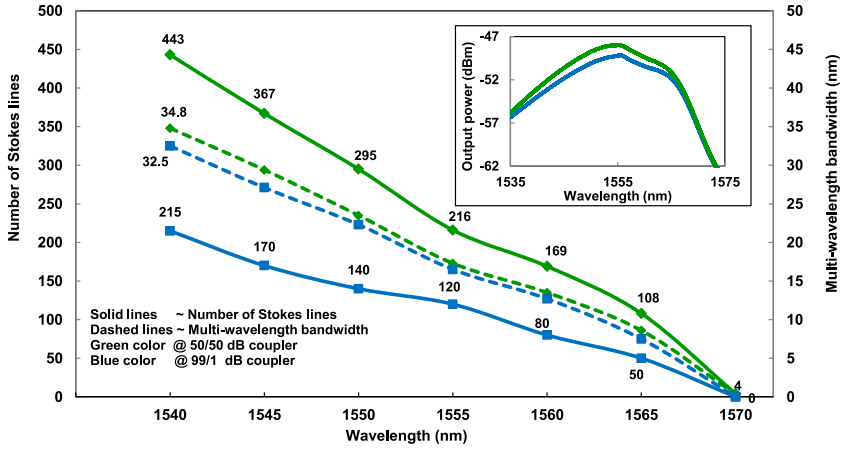

Fig. 6. Variations of multi-wavelength bandwidth and number of channels measured at OSA1 against the BP wavelengths (RPP = 1000 mW, BP power = −2.6 dBm). The inset graph is the ASE spectra for 50/50 and 99/1 couplers when the RPP is set at 1000 mW and the BP signal is switched off.

maintained at the optimum value of −2.6 dBm. From this Fig., the bandwidth and number of channels are inversely proportional to the BP wavelength for both coupling ratios since the residual Raman gain bandwidth becomes narrower [6]. This is better understood by referring to the amplified spontaneous emission (ASE) noise at both coupling ratios as depicted in the inset of Fig. 6. The characterization is done when the RPP is set at 1000 mW with the absence of BP signal. The curve feature explains the maximum attainment of lasing lines at 1540 nm BP wavelength but not at that relates to the Raman peak gain. In fact, the continuous decline in the number of channels is realized although the spectral power remains similar for the entire BP wavelength range. When employing the 3-dB coupler that induces single-wavelength spacing, a maximum of 443 Stokes lines is attained with considerably uniform peak power. These are produced over 34.8 nm bandwidths when the BP wavelength is set at 1540 nm as depicted in Fig. 7. In contrast for the 99/1 coupler that results in double-wavelength spacing, maximum Stokes lines of 215 are achieved over 32.5 nm bandwidths

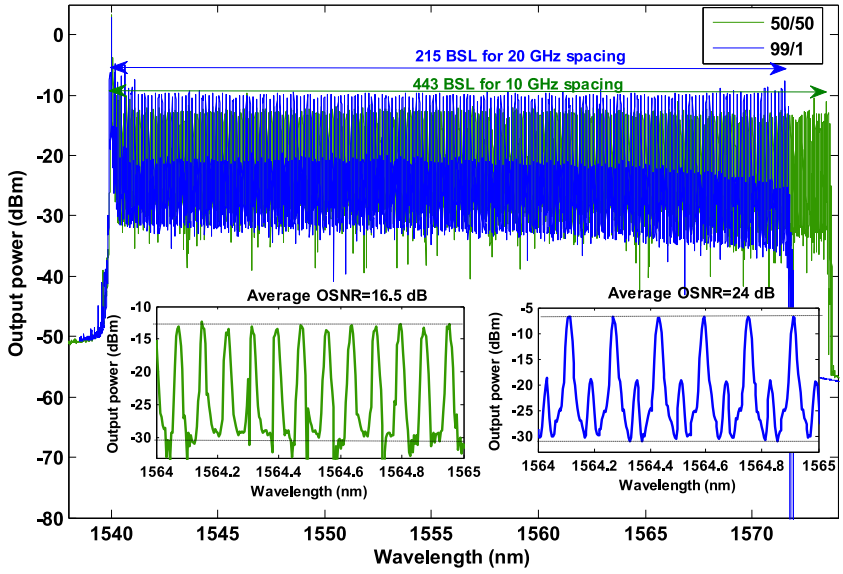

Fig. 7. Representation for spectral combs described in Fig. 6 with 10 GHz spacing (50/50) and 20 GHz spacing (99/1) with inset graphs that relate to their enlarged views (BP wavelength = 1540 nm, RPP = 1000 mW, BP power = −2.6 dBm).

at the same BP wavelength (see Fig. 7). The optimum number of lasing lines cannot be generated when the BP wavelength is detuned to the region of lower than 1540 nm for both coupling ratios. This is because at a shorter wavelength span, more energy is required for the initiation of wider multi-channel lasing bandwidth. This latter attribute is influenced by the wavelength dependencies on BP and stimulated Raman scattering (SRS) bandwidths. A higher Raman gain might broaden the SRS bandwidths, however the build-up of self-lasing cavity modes cannot be efficiently suppressed at this band-edge due to the lower property of Raman gain. This validates the limitation in wavelength operation as shown in Fig. 6. Besides this, it can be claimed that by employing a 50/50 coupler, the ASE spectrum shows a higher gain profile in comparison to that when a 99/1 coupler is applied. A higher Raman gain leads to a more energy transfer from Raman pump waves to the BSL which may result in increments of the number of channels and multi-wavelength bandwidth as well. This proves the multi-wavelength bandwidth enhancement as observed in the 50/50 coupler (see green and blue dashed lines in Fig. 6).

For a visual study, their spectral features are illustrated in Fig. 7 together with the corresponding magnified profiles that are included in the inset graphs. From this Fig., it can be seen that employing the 50/50 coupler also yields an average output peak power of −13.5 dBm and 16.5 dB OSNR. Although, excellent results in [5] present over 500 Stokes lines at 10 GHz spacing across 40 nm bandwidth, it suffers from diminished OSNR and low output peak power. On the contrary, the employment of 99/1 coupler produces an average of −9 dBm output peak power with 24 dB OSNR. In this case, its lasing performances are comparable to our previous study for 20 GHz spacing that produces 212 BSL over 29 nm wavelength range [7]. On the other hand, we need to emphasize that the generated Stokes in OSA1 and OSA 2 in this study are completely different to the results achieved in [8]. This is because the generation of 10 and 20 GHz spacing in a single cavity dimension are produced through overlapping effects in opposite directions inside the variable optical coupler. The feedback is initiated by multiple Rayleigh scattering and efficient operation is achieved up to a Watt pump power level. However, the feedback in our previous assessment [8] is attained through a reflective mirror at port 2 which leads to 10 GHz. spacing at all pump-coupling distribution. When incorporating a 99/1 coupler, the optimized operation is satisfied at just a few hundreds mW RPP. As a result, a maximum of 28 lasing lines are realized with 17 dB OSNR. In summary, the results achieved in this paper offer superior advantages especially enhanced flexibility

and functionality due to switchable wavelength spacing capability. To date, no any report on this topic is available for comparison when implementing MBRFL structure except in [21] where less than 20 Stokes and anti-Stokes lines are generated at both wavelengths spacing operation. Other favorable properties include reasonably tunable and wide multi-wavelength bandwidth, high number of channels with good OSNR and high Stokes peak power in comparison with other previous works [5]–[8], [3]–[15], [17], [21], [22]. It is noted that, the results achieved in [23]–[25] shows tunable multi-wavelength fiber lasers from different gain media. The generated Stokes attributes with regards to number of channels ($\leq$16) and multi-wavelength bandwidth ($\sim$2 nm) are not comparable to our results. In addition, there is no development for switchable MBRFL in the C band with high quality properties. So to the best of our knowledge, our scheme resolves previous problems for MBRFL especially with respect to wavelength operation, Stokes peak power, and complexity.

4. Conclusion

The novelty of this work is the utilization of a NAFL structure with various coupling ratio as a decisive elements in determining the wavelength spacing between the BSL. The main objective of generating switchable wavelength operation from 10 to 20 GHz with outstanding performances through a simple arrangement has been successfully fulfilled. The incorporation of a 50/50 coupler satisfies the generation of single-wavelength spacing due to its minimum destructive interference. In addition, when the CR is set at 99/1, double-wavelength spacing is produced due to its maximum destructive interference. Our achievements present excellent lasing performances such as high number of channels, good OSNR, and high Stokes peak power. Other remarkable qualities include wide multi-wavelength bandwidth as well as wavelength tunability. In conclusion, better understanding of these physical insights might introduce a more improved version of this class of laser that is favorable for multiple channels applications that include optical communication and sensing.

References

[1] M. H. Al-Mansoori and M. A. Mahdi, "Multi-wavelength L-band Brillouin–Erbium comb fiber laser utilizing nonlinear amplifying loop mirror," *J. Lightw. Technol.*, vol. 27, no. 22, pp. 5038–5044, Nov. 2009.

[2] N. Shahabuddin, H. Ahmad, Z. Yusoff, and S. W. Harun, "Spacing-switchable multi-wavelength fiber laser based on nonlinear polarization rotation and Brillouin scattering in photonic crystal fiber," *IEEE J. Photon.*, vol. 4, no. 1, pp. 34–38, Feb. 2012.

[3] A. Al-Alimi, M. H. Yaacob, and A. F. Abas, "Nonlinear fiber loop mirror optimization to enhance the performance of multi-wavelength Brillouin/Erbium-Doped fiber laser," *IEEE J. Photon.*, vol. 6, no. 6, pp. 1–10, Dec. 2014.

[4] B. Min, P. Kim, and N. Park, "Flat amplitude equal spacing 798-channel Rayleigh-assisted Brillouin/Raman multi-wavelength comb generation in dispersion compensating fiber," *IEEE Photon. Technol. Lett.*, vol. 13, no. 12, pp. 1352–1354, Dec. 2001.

[5] Z. Wang, Z. Wu, H. Fan, M. Li, Y. Yuan, and R. Yunjiang, "Broadband flat-amplitude multi-wavelength Brillouin-Raman fiber laser with spectral reshaping by Rayleigh scattering," *Opt. Exp.*, vol. 21, pp. 29358–29363, 2013.

[6] G. Mamdoohi, A. R. Sarmani, A. F. Abas, M. Mokhtar, M. H. Yaacob, and M. A. Mahdi, "20 GHz spacing multi-wavelength generation of Brillouin-Raman fiber laser in a hybrid linear cavity," *Opt. Exp.*, vol. 21, pp. 18724–18732, 2013.

[7] G. Mamdoohi, A. R. Sarmani, A. F. Abas, M. Mokhtar, M. H. Yaacob, and M. A. Mahdi, "Effects of Raman pump power distribution on output spectrum in a multi-wavelength BRFL," *Opt. Exp.*, vol. 23, pp. 29127–29127, 2015.

[8] G. Mamdoohi, A. R. Sarmani, A. F. Abas, M. Mokhtar, M. H. Yaacob, and M. A. Mahdi, "Multi-wavelength Brillouin-Raman fiber laser utilizing enhanced nonlinear amplifying loop mirror design," *Opt. Exp.*, vol. 21, pp. 31800–31808, 2013.

[9] A. K. Zamzuri, M. I. Md Ali, A. Ahmad, R. Mohamad, and M. A. Mahdi, "Brillouin-Raman comb fiber laser with cooperative Rayleigh scattering in a linear cavity," *Opt. Lett.*, vol. 31, pp. 918–920, 2006.

[10] A. K. Zamzuri, M. A. Mahdi, A. Ahmad, M. I. Md A, and M. H. Al-Mansoori, "Flat amplitude multi-wavelength Brillouin-Raman comb fiber laser in Rayleigh-scattering-enhanced linear cavity," *Opt. Exp.*, vol. 15, pp. 3000–3005, 2007.

[11] R. S. Shargh, M. H. Al-Mansoori, S. B. A. Anas, R. K. Z. Sahbudin, and M. A. Mahdi, "OSNR enhancement utilizing large effective area fiber in a multi-wavelength Brillouin-Raman fiber laser Laser," *Laser Phys. Lett.*, vol. 8, pp. 139–143, 2011.

[12] A. K. Zamzuri *et al.*, "OSNR variation of multiple laser lines in Brillouin-Raman fiber laser," *Opt. Exp.*, vol. 17, pp. 16904–16910, 2009.

[13] H. Ahmad, M. Z. Zulkifli, N. A. Hassan, and S. W. Harun, "S-band multi-wavelength ring Brillouin/Raman fiber laser with 20 GHz channel spacing," *Appl. Opt.*, vol. 51, pp. 1811–1815, 2012.

[14] N. A. M. A. Hambali, M. H. Al-Mansoori, M. Ajiya, A. A. Bakar, S. Hitam, and M. A. Mahdi, "Multi-wavelength Brillouin-Raman ring-cavity fiber laser with 22-GHz spacing," *Laser Phys.*, vol. 21, pp. 1656–1660, 2011.

[15] A. Abass, M. H. Al-Mansoori, M. Z. Jamaludin, F. Abdullah, T. F. Al-Mashhadani, and M. H. Ali, "L-Band multi-wavelength Brillouin–Raman fiber laser with 20-GHz channel spacing fiber," *Integrated Opt.*, vol. 33, pp. 56–67, 2014.
[16] Y. Liu, G. D. Wang, and X. Dong, "Stable room-temperature multi-wavelength lasing oscillations in a Brillouin–Raman fiber ring laser," *Opt. Commun.*, vol. 281, pp. 5400–5404, 2008.
[17] H. Ahmad, M. Z. Zulkifli, S. F. Norizan, M. H. Jemangin, and S. W. Harun, "S-band multi-wavelength Brillouin Raman fiber laser," *Opt. Commun.*, vol. 284, pp.4971–4974, 2011.
[18] S. Boscolo, R. Bhamber, and S. K. Turitsyn, "Design of Raman-based nonlinear loop mirror for all-optical 2R regeneration of differential phase-shift-keying transmission," *IEEE J. Quantum Electron.*, vol. 42, no. 7, pp. 619–624, Jul. 2006.
[19] G. Agrawal, *Applications of Nonlinear Fiber Optics*. San Diego, CA, USA: Academic, 2001.
[20] S. A. Babin, D. V Churkin, A. E. Ismagulov, S. I. Kablukov, and E. V. Podivilov, "Four-wave-mixing-induced turbulent spectral broadening in a long Raman fiber laser," *JOSA B*, vol. 24, pp. 1729–1738, 2007.
[21] M. Shirazi, M. J. Taib, K. Dimyati, S. W. Harun, and H. Ahmad, "Multi-wavelength Brillouin–Raman fiber laser generation assisted by multiple four-wave mixing processes in a ring cavity," *Laser. Phys.*, vol. 23, pp. 075108–075116, 2013.
[22] H. Wu *et al.*, "Flat amplitude multi-wavelength Brillouin–Raman random fiber laser with a half-open cavity," *Appl. Phys. B.*, vol. 112, pp. 467–471, 2013.
[23] X. Zhou, K. Hu, Y. Wei, M. Bi, and G. Yang, "An L-band multi-wavelength Brillouin–Erbium fiber laser with switchable frequency spacing," *Laser Phys.*, vol. 27, pp. 015103–015108, 2016.
[24] L. Qian, D. Fen, H. Xie, and J. Sun, "A novel tunable multi-wavelength Brillouin fiber laser with switchable frequency spacing," *Opt. Commun.*, vol. 340, pp. 74–79, 2015.
[25] P. Zhang, T. Wang, Q. Jia, and K. Dong, "L-band double Brillouin frequency spaced tunable multi-wavelength Brillouin fiber laser," in *Proc. Int. Symp. Optoelectron. Technol. Appl.*, 2014, vol. 9294, pp. 1–4.